



HAL
open science

Ultraflexible Glassy Semiconductor Fibers for Thermal Sensing and Positioning

Ting Zhang, Zhe Wang, Bhuvanesh Srinivasan, Zhixun Wang, Jing Zhang, Kaiwei Li, Catherine Boussard-Plédel, Johann Troles, Bruno Bureau, Lei Wei

► **To cite this version:**

Ting Zhang, Zhe Wang, Bhuvanesh Srinivasan, Zhixun Wang, Jing Zhang, et al.. Ultraflexible Glassy Semiconductor Fibers for Thermal Sensing and Positioning. ACS Applied Materials & Interfaces, 2019, 11 (2), pp.2441-2447. 10.1021/acsami.8b20307 . hal-01971819

HAL Id: hal-01971819

<https://univ-rennes.hal.science/hal-01971819>

Submitted on 7 Jan 2019

HAL is a multi-disciplinary open access archive for the deposit and dissemination of scientific research documents, whether they are published or not. The documents may come from teaching and research institutions in France or abroad, or from public or private research centers.

L'archive ouverte pluridisciplinaire **HAL**, est destinée au dépôt et à la diffusion de documents scientifiques de niveau recherche, publiés ou non, émanant des établissements d'enseignement et de recherche français ou étrangers, des laboratoires publics ou privés.

Ultra-Flexible Glassy Semiconductor Fibers for Thermal Sensing and Positioning

Ting Zhang,^{†,§} Zhe Wang,^{†,§} Bhuvanesh Srinivasan,[‡] Zhixun Wang,[†] Jing Zhang,[†] Kaiwei Li,[†] Catherine Boussard-Pledel,[‡] Johann Troles,[‡] Bruno Bureau[‡] and Lei Wei^{,†}*

[†]School of Electrical and Electronic Engineering, Nanyang Technological University, 50 Nanyang Avenue, 639798, Singapore

[‡]Institut des Sciences Chimiques de Rennes, UMR CNRS 6226, University of Rennes, F-35000 Rennes, France

KEYWORDS: thermoelectric fibers, fiber fabrication, glassy semiconductors, thermal sensors, mechanical flexibility, wearable electronics

ABSTRACT

Flexible, large-area, and low-cost thermal sensing network with high spatial and temporal resolution are of profound importance in addressing the increasing needs for industrial processing, medical diagnosis, and military defense. Here, a thermoelectric fiber is fabricated by thermally co-drawing of a macroscopic preform containing semiconducting glass core and polymer cladding to deliver thermal sensor functionalities at fiber-optic length scales, flexibility, and uniformity. The resulting thermoelectric fiber sensor operates in a wide temperature range with high thermal detection sensitivity and accuracy, while offering ultra-flexibility with the

1
2
3 bending curvature radius below 2.5 mm. Additionally, a single thermoelectric fiber can either
4 sense the spot temperature variation or locate the heat/cold spot on the fiber. As a proof-of-
5 concept, a two-dimensional 3×3 fiber array is woven into a textile to simultaneously detect the
6 temperature distribution and the position of heat/cold source with the spatial resolution of
7 millimeter. Achieving this may lead to the realization of large-area, flexible and wearable
8 temperature sensing fabrics for wearable electronics and advanced artificial intelligence
9 applications.
10
11
12
13
14
15
16
17
18

19 20 **1. Introduction**

21
22
23 Thermal sensor, a component to monitor the temperature, reveals the important information
24 about the dynamics of many chemical, physical and biological phenomena,¹ and acts as one of
25 the most frequently employed sensors for industrial processing, medical diagnosis, military
26 defense, etc. Typical thermal sensors are based on thermistors, thermoelectrics or infrared
27 radiation (IR).²⁻⁴ IR-imaging systems have been widely applied in the situations where line-of-
28 sight contact can be made between the measured object and the camera lens, however, it is still
29 challenging to develop flexible thermal sensor to detect the thermal excitation on a large area
30 with the consideration of the irregularity of the monitored surface, spatial constraints, or cost.^{1,5}
31 For instance, the recent development on electronic skin and wearable devices requires such a
32 thermal sensing network with high-spatial resolution to monitor the human body temperature or
33 provide the information of thermal distribution for robotics,⁶⁻⁹ that can conformably wrap
34 irregular surfaces and spatially quantify temperature. Achieving this may further enable the
35 advanced artificial intelligence applications.
36
37
38
39
40
41
42
43
44
45
46
47
48
49
50
51
52
53
54
55
56
57
58
59
60

1
2
3 Within thermoelectric (TE) technology, the Seebeck effect states that charge carriers
4 thermally diffuse in a TE material under a temperature difference, resulting in an output voltage
5 proportional to the temperature difference multiplied by the Seebeck coefficient of the material.
6
7
8
9
10-12 Thus, this effect can also be utilized to monitor temperature variation according to the
11 corresponding output voltage, and has long been adopted in thermocouple applications.^{13, 14} The
12 sensitivity of thermal sensor can be evaluated by how fast and how large such voltage generation
13 occurs from a minimal temperature change. Hence, very large Seebeck coefficients of thermal
14 sensors based on TE materials are critical in applications that require highly sensitive and
15 accurate measurements of temperature. Recently, the studies on bulk semiconducting glasses of
16 the quaternary Cu–As–Te–Se system demonstrate that these semiconducting glasses possess a
17 large Seebeck coefficient ranging from 400 to 1100 $\mu\text{V}/\text{K}$ in spite of a low TE figure of merit,¹⁵⁻
18
19
20
21
22
23
24
25
26
27
28
29
30
31
32
33
34
35
36
37
38
39
40
41
42
43
44
45
46
47
48
49
50
51
52
53
54
55
56
57
58
59
60

flexible high-performance TE fiber for thermal sensing and positioning.

Multimaterial fibers integrate a multiplicity of functional components into one fiber to share the basic device attributes of their traditional bulk counterparts, yet are fabricated using conventional preform-based fiber-processing methods, yielding kilometers of flexible functional fiber devices which can be also assembled to large-scale and flexible multifunctional fabrics.²²⁻²⁶ Here, we present the realization of thermal sensing in arbitrarily long and flexible fiber-like devices by thermally co-drawing semiconducting glass as the core and thermoplastic polymer as the cladding. The resulting TE fibers exhibit large Seebeck coefficients and high thermal conductivity, working as a thermal sensor in a wide temperature range up to 150 °C with the

1
2
3 measurement resolution as high as 0.05 °C. We characterize the sensing performance of a single
4 TE fiber via monitoring the temperature change of a thermal source at the fixed point of the fiber
5
6 or detecting the different points of a thermal source on the fiber with the fixed temperature. To
7
8 monitor and position a heat/cold source at the same time, a two-dimensional fiber array with the
9
10 grid size of 24 mm×24 mm is constructed. Importantly, the fiber-to-fabric nature of such a
11
12 thermal sensing array requires only a $2N$ number of fibers to achieve N^2 detection resolution,
13
14 enabling the applications related but not limited to large-area thermal sensing and positioning.
15
16
17
18
19

20 **2. Results and discussion**

21
22
23 Preform-to-fiber fabrication by thermal drawing technique requires the glass transition
24
25 temperatures of the supporting materials to be slightly higher than the melting points of the
26
27 functional materials to support the draw stress, while continuously and controllably pulling the
28
29 macroscopic preform down to microscopic fiber. However, inorganic TE materials with high TE
30
31 performance such as Bi_2Te_3 , SnSe and SiGe alloys normally have high melting points and can
32
33 only be drawn with glass cladding,¹⁰ resulting a compromised flexibility. To achieve ultra-
34
35 flexible TE fibers, we adopt an amorphous semiconducting glass as the TE core material and a
36
37 thermoplastic polyetherimide (PEI) polymer with high flexibility as the cladding material.
38
39
40
41

42
43 Figure 1a schematically shows the preform-based fabrication of TE fibers. A
44
45 semiconducting glass rod of $(\text{Te}_{85}\text{Se}_{15})_{45}\text{As}_{30}\text{Cu}_{25}$ shown in the inset of Figure 1a is first
46
47 synthesized by standard sealed-ampoule technique^{15,16} and the detailed processes are described in
48
49 the following Experimental Section. This semiconducting glass offers two superior properties in
50
51 constructing flexible thermal sensors. One is that its Seebeck coefficient is large enough to
52
53 ensure the sensitivity of thermal sensing. The other is that its glass transition temperature (T_g) is
54
55
56
57
58
59
60

1
2
3 170 °C and crystallization temperature (T_c) is 270 °C, as measured in Figure 1b, offering a wide
4 glass stability range of 100 °C, which makes it particularly suitable for the thermal fiber drawing
5 process with the polymer matrix. Then, PEI polymer with the softening temperature of 217 °C is
6 used to support and confine $(\text{Te}_{85}\text{Se}_{15})_{45}\text{As}_{30}\text{Cu}_{25}$, while providing excellent mechanical
7 properties as shown in Figure S1. The plastic stress of pure PEI fiber exceeds 90 Mpa, and the
8 elastic strain confines 10 %. To increase the contact area between heat source and TE fiber as
9 well as reduce the heat loss between heat source and semiconducting glass core, we machine a
10 hollow rectangular-shaped PEI blocks with the cross section of 20 mm×8 mm and the diameter
11 of central hollow channel is 4 mm. The synthesized semiconducting glass is reshaped and filled
12 in the hollow PEI block, and then the entire assembly is thermally sealed in the vacuum oven to
13 form an all-solid macroscopic preform. The preform is further loaded in a fiber draw tower with
14 a narrow heating zone, and thermally drawn at the temperature of 250 °C, where the viscosity of
15 the PEI cladding is much larger than that of the TE glass core, thus supporting the whole
16 structure and yielding hundreds of meters of TE fibers.

17
18
19
20
21
22
23
24
25
26
27
28
29
30
31
32
33
34
35
36 Figure 1c shows the photograph of the resulting TE fiber and its optical microscope image
37 of the cross-section. Owing to the presence of polymer cladding, the resulting fiber exhibits high
38 mechanical flexibility to be easily bent, coiled and woven. The continuous semiconducting glass
39 core and polymer cladding are well maintained in round and rectangular shape respectively, and
40 the interfaces between core and cladding are clearly defined. The diameter of the fiber core is
41 near 400 μm and the overall fiber dimension of 1.87 mm×0.75 mm, which approaches the same
42 dimension ratio of the materials in the original preform, demonstrating that such a thermal
43 drawing is a physically proportional size-reduction process. The required TE fiber dimension can
44 be precisely controlled via adjusting the feeding speed of the preform and the drawing speed of
45
46
47
48
49
50
51
52
53
54
55
56
57
58
59
60

1
2
3 the fiber. For examining the components of TE fiber, the energy dispersive X-ray (EDX)
4 mappings results in Figure 1d demonstrate that the functional glass core are consisted of Cu–As–
5 Te–Se quaternary system and stably confined in the polymer cladding without diffusion or
6 chemical reaction during the drawing process. Moreover, the EDX spectra of Figure S2 show
7 that the atomic ratio of Te:Se:As:Cu in the fiber core is about 39:6:30:25, which is close to
8 $(\text{Te}_{85}\text{Se}_{15})_{45}\text{As}_{30}\text{Cu}_{25}$ and consistent with the original composition of the semiconducting glass in
9 the preform.

10
11
12
13
14
15
16
17
18
19
20 TE properties of the semiconducting glass depends on its crystal structure. Wide-angle X-ray
21 scattering (WAXS) is taken to confirm the crystal structure of the fiber core after etching the PEI
22 cladding using dichlormethane solution. The X-ray diffraction spectrum in Figure 2a and WAXS
23 image in Figure S3a indicate the amorphous nature of the semiconducting core in the drawn TE
24 fiber though minor crystallization peaks of As and Cu_2As phases appear. For comparison, the TE
25 fiber is also crystallized by heating it to 300 °C for 3 hours and then cooling to room temperature
26 in a vacuum oven. Figure 2a and Figure S3b clearly reveal its crystal peaks of X-ray diffraction
27 spectrum and diffraction ring in the WAXS image, which are not in presence of our original
28 drawn TE fibers. For amorphous state, as shown in Figures 2b-d, the TE glass shows that the
29 Seebeck coefficients (S) decrease from 523 to 477 $\mu\text{V}/\text{K}$ with the measured temperature from
30 300 K to 420 K, while the electrical conductivities (σ) increase from 9.24 to 98.15 S/m, leading
31 to the power factors ($S^2\sigma$) enhanced from 2.52 to 22.36 $\mu\text{W}/\text{mK}^2$. However, the thermal
32 conductivities are around 4.0 W/mK in the experimental temperature range (Figure 2e) and
33 higher than the reported thermal conductivities of the amorphous Cu–As–Te–Se glasses.^{15,16}
34 This can be explained by the emergence of crystalline phases, as the minor crystal peaks in the
35
36
37
38
39
40
41
42
43
44
45
46
47
48
49
50
51
52
53
54
55
56
57
58
59
60

1
2
3 X-ray diffraction spectrum in Figure 2a, which will increase the thermal conductivity and
4
5 decrease the final TE Figure of merit (ZT) as shown in Figure 2f.
6
7

8
9 Compared with amorphous state, the Seebeck coefficient of crystalline fiber core decreases
10 while the electrical conductivity increases due to the formed Cu-Te and Cu-Se bonds,¹⁷ which
11 results in a higher power factor and TE figure of merits ZT of crystalline semiconducting fiber
12 core in a temperature ranging from 300K to 400K. However, for thermal sensing property, we
13 need large Seebeck coefficients to guarantee high sensitivity and accuracy of thermal sensor,
14 where a fast and large voltage generation occurs from a minimal temperature change. Therefore,
15 the crystalline fiber core can improve the thermoelectric properties^{15,16} and suitable for power
16 generation, but the amorphous fiber core possesses higher Seebeck coefficients and lower
17 thermal conductivities, and can be more applicable for thermal sensor.
18
19
20
21
22
23
24
25
26
27
28
29

30 When the resulting fibers act as thermal sensors, the measuring principle for a single TE
31 fiber is schematically shown in Figure 3a. Based on the Seebeck effect, when a heat source is
32 applied to the TE fiber, the temperature difference between the two ends of the fiber is
33 established, which causes the hole carrier diffusion in semiconductor glass core and generates the
34 voltage outputs via copper electrodes. Figure 3b records the real-time temperature change of the
35 heat source located on the 20% length of the entire fiber, and plots the output voltage from the
36 temperature difference at two fiber ends. As the temperature of heat source increases from room
37 temperature of 25 °C, the corresponding output voltage increases rapidly with the sampling
38 duration of 500 ms and the temperature resolution is higher than 0.05 °C (Figure 3c). The
39 accuracy and sensitivity are comparable with most of the commercial thermal sensors. The inset
40 in Figure 3b indicates the output voltage increases lineally with the raised temperature of the heat
41 source with fixed location. Considering that the location of heat source affects the temperature
42
43
44
45
46
47
48
49
50
51
52
53
54
55
56
57
58
59
60

1
2
3 gradient and output voltage between the two ends of the fiber, we further characterize the heat
4 source position of a single TE fiber by touching different locations of the fiber with one finger
5 around 35 °C, as plotted in Figure 3d. At the central position of the fiber namely 50% fiber
6 length, the heat of a finger equally transfers from the central position to both ends, and there is a
7 small temperature difference at the two ends of the fiber, resulting in a weak output voltage. As
8 the finger moves from the central position to the fiber end, the output voltage increases
9 exponentially, and the positive or negative values are symmetrical with the middle point,
10 indicating that a single TE fiber is capable of positioning the heat source, rather than simply
11 detecting the temperature.¹ More importantly, the response time is very fast and only needs three
12 seconds for the finger touch to reach steady state (Figure 3e). Besides its high thermal sensing
13 performance, we also study its flexibility, as summarized in Figure 3f. The curvature radius
14 decreases largely when the fiber thickness reduces. Even for a thick fiber with the thickness of
15 0.6 mm, the curvature radius is still less than 2.5 mm, which is more flexible in contrast to the
16 TE fiber with the glass cladding.¹⁰ The inset in Figure 3f exhibits that the fiber sensor is flexible
17 enough to be easily wrapped on the glass rod surface with the diameter of 3 mm, without
18 compromising its high thermal sensing performance. Thus, it is a promising candidate to
19 fabricate large-area, flexible and wearable temperature sensing fabrics.
20
21
22
23
24
25
26
27
28
29
30
31
32
33
34
35
36
37
38
39
40
41
42

43 The thermal sensing performance of TE fiber mainly depends on the temperature gradient
44 and electric potential distribution in the semiconducting glass core owing to the Seebeck effect.
45 Using the finite element simulation where all the parameters and the geometries of the TE fibers
46 are defined to be close to the actual materials and structures, we theoretically evaluate the
47 temperature gradient and electric potential distribution in a single TE fiber, as shown in Figure
48 4a. The environment temperature is set to be 25 °C, while the temperature of heat source is 36
49
50
51
52
53
54
55
56
57
58
59
60

1
2
3 °C. When the heat source is placed on the fiber surface of 16.5% length, the output voltage on the
4 fiber end is 504 μV , and the output voltage decreases exponentially and symmetrizes with the
5 middle point (Figure 4b) as the thermal source moves from one end to the other end, which has
6 the same tendency as the experimental results. Figure 4c gives the output voltages induced by
7 different temperatures on the middle point, 15% and 85% fiber length points, respectively. The
8 output voltage of the middle point is almost zero and constant with the increased temperature,
9 while the absolute values of output voltage for 15% and 85% fiber length points is identical
10 under the same temperature and increase with the raised temperature due to their symmetry.
11 These results fully prove that a single TE fiber can sense the temperature variation of a fixed spot
12 or position the spot location under a specific temperature applied on the fiber. In principle, the
13 more proportion of semiconducting glass core in the thickness direction of the fiber occupies, the
14 higher thermal sensing performance of the fiber presents, because thinner polymer cladding
15 lowers the heat loss and thicker semiconducting glass core enhances electrical and thermal
16 conductivity. However, large proportion of semiconducting glass core will sacrifice the fiber's
17 flexibility. Figure 4d illustrates the simulated output voltages and deflections of the fiber thermal
18 sensor for different thickness ratios between the semiconducting glass core and the entire fiber.
19 The temperature of heat source is still 36 °C and the location is at 22.2% fiber length. The results
20 indicate that, as the proportion of semiconducting glass core increases, the sensitivity of fiber
21 sensor is improved yet the flexibility is weakened. The optimized proportion is about 50% ~
22 60%, which approaches the similar dimension of our fabricated TE fibers.

23
24
25
26
27
28
29
30
31
32
33
34
35
36
37
38
39
40
41
42
43
44
45
46
47
48
49
50 Although single TE fiber is able to sense the temperature with fixed location or position the
51 thermal source with fixed temperature by the output voltage, it is hard to obtain both the
52 temperature and the location of thermal source. For instance, an output voltage of 2.5 mV may
53
54
55
56
57
58
59
60

1
2
3 be from the heat source with the temperature of 36 °C and the location of 5 % fiber length
4 (Figure 4b) or the temperature of 80 °C and the location of 15 % fiber length (Figure 4c). To
5
6 address this challenge, here we construct a flexible thermal sensor network based on a 3×3 TE
7
8 fiber array woven into a flexible textile as a prototype to obtain spatially resolved thermal
9
10 information including both thermal sensing and positioning. The 3×3 thermal sensor array with
11
12 the grid size of 24 mm × 24 mm is assembled by six TE fibers with length of 8 cm, as shown in
13
14 the left image of Figure 5a. By touching the fiber network with the finger at different points as
15
16 marked with capital letters in the right image of Figure 5a, and analyzing all the output voltages
17
18 of the six fibers from V_1 to V_6 as plotted in Figure 5b, the distinguishable voltage signal from
19
20 each grid axis can reveal the accurate position and temperature of the finger. Moreover, if fiber 1
21
22 and fiber 2 are regarded as Y-axis and X-axis respectively, we can locate the quadrant of the
23
24 thermal source by the sign of the distinguishable voltage. For instance, the finger touching point
25
26 E shown in Figure 5a is resolved in the second quadrant and at the cross point of fiber 3 and fiber
27
28 4, owing to a positive voltage form fiber 3 and a negative voltage form fiber 4. Furthermore, the
29
30 accurate temperature of the finger is determined by the largest output voltage values of a single
31
32 fiber sensor that we discussed above. Beyond these results, we also find that the absolute value
33
34 of output voltage from fiber 4 is a bit higher than that from fiber 3 located in thermal point E on
35
36 the same position of both fiber 3 and fiber 4, which is mainly caused by the heat loss from the
37
38 upper fiber 4 to the bottom fiber 3. Interestingly, this difference can be utilized to detect the
39
40 pointing direction of the thermal source, for example in this case, the heat points from the upper
41
42 side to the bottom side of the fiber network. As a comparison, we present both a thermal IR
43
44 image taken by an IR camera (FLIR C2) and a reconstructed thermal map using the data obtained
45
46 from the fiber array for two situations. One is the finger heating with the temperature of 33 °C
47
48
49
50
51
52
53
54
55
56
57
58
59
60

1
2
3 and the other is the ingot cooling with the temperature of 22 °C, as displayed in Figures 5c to 5e.
4
5 These results confirm the capability of the TE fiber array for ultra-flexible and large-area
6
7 detecting, localizing and monitoring the thermal source with high spatially temperature
8
9 resolution.
10

11 12 13 **3. Conclusions**

14
15
16 In summary, an ultra-flexible thermal sensor is fabricated by thermally co-drawing
17
18 semiconducting glass core and polymer cladding into a TE fiber. This fabrication technique
19
20 delivers TE fiber functionalities at fiber-optic length scales, flexibility, uniformity and cost. Both
21
22 theoretical and experimental results suggest that the resulting single TE fiber is capable to
23
24 detect thermal source in a wide temperature range up to 150 °C with the measurement
25
26 resolution as high as 0.05 °C, and locate thermal source with the resolution of millimeter.
27
28 Furthermore, a flexible thermal sensor network by 3×3 TE fiber arrays is experimentally applied
29
30 for simultaneously realizing thermal sensing and positioning with high spatially resolution.
31
32 Hence, the demonstrated flexible thermal sensing fiber may lead to the important applications in
33
34 thermometry, thermography, smart sensors, robotics' e-skin, health-monitoring products and
35
36 wearable electronics.
37
38
39
40

41 42 43 **4. Experimental Section**

44
45 **Semiconducting glass synthesis:** The chalcogenide glass rods of the quaternary
46
47 $(\text{Te}_{85}\text{Se}_{15})_{45}\text{As}_{30}\text{Cu}_{25}$ with diameters of 7 mm and several centimeters in length are prepared from
48
49 high-purity (5–6N) As, Te, Se and Cu elements (Sigma Aldrich) using sealed-ampoule melt-
50
51 quenching techniques. The materials are weighted proportionally and placed into a quartz tube
52
53 under nitrogen atmosphere. The tube is cleaned with hydrofluoric acid and then heated to 330 °C
54
55
56
57
58
59
60

1
2
3 for an hour at a rate of 1 °C/min under vacuum in order to remove surface oxides. The ampoule
4 is formed by sealing the tube under vacuum of 10^{-5} Torr. It is then heated to 850 °C at a rate of 2
5
6 °C/min in a rocking furnace for 8 hours. The homogeneous glass liquid is cooled to 600 °C in the
7
8 rocking furnace and held for 45 mins before quenching the glass in cold water. Subsequently, the
9
10 glass tubes are readily annealed near T_g of 170 °C for 3 hours.
11
12
13

14
15 ***Fabrication of flexible TE fibers:*** Hundreds of meters of fiber are obtained from a
16
17 macroscopic rectangular preform with the sectional area of 20 mm×8 mm, which consists of the
18
19 semiconducting glass core with a reshaped diameter of 4 mm and the protective PEI polymer
20
21 cladding. Then the assembled preform is consolidated for 60 mins at 230 °C under vacuum (10^{-3}
22
23 Torr) to remove the trapped gas and form high quality interfaces. Finally, the preform is
24
25 thermally drawn in a two-zone vertical tube furnace with the top-zone temperature 150 °C and
26
27 the bottom-zone temperature 250 °C respectively to obtain the microscopic fibers.
28
29
30

31
32 ***Characterization:*** The morphologies and components of TE fibers are examined by digital
33
34 microscopy (Olympus BX51) and field emission scanning electron microscope (FESEM, JEOL
35
36 7600F) equipped with energy dispersive X-ray (EDX) where the TE fibers are firstly embedded
37
38 into an epoxy matrix and polished into a smooth cross section by a polishing machine. The
39
40 crystal structures of TE fiber cores are analyzed with X-ray diffractometer (Xenocs Nano-
41
42 inXider) after releasing them from the fiber by dissolving PEI cladding in dichlormethane
43
44 solution. The glass transition temperature T_g and crystallization temperature T_x of the
45
46 semiconducting glass core are measured using a differential scanning calorimeter (DSC Q1000)
47
48 at a heating rate of 10 °C /min. Both Seebeck coefficient and electrical resistivity of the glass
49
50 core are carried out by a ULVAC ZEM-3, while the thermal conductivities are measured under
51
52 an argon atmosphere using a laser flash (Netzsh LFA 447). As for the thermal sensing test of
53
54
55
56
57
58
59
60

1
2
3 single TE fiber, a Keithley 2602B source measure unit is used to power the heat for changing
4 temperature of thermal source, meanwhile a Keithley 2182A nanovoltmeter connecting with two
5 copper electrodes measures the output TE voltage and a Keithley 2700 multimeter records the
6 temperature data. The output voltages from thermal sensor network are collected by multi-
7 channel data acquisition card of Keithley 7700. A multi-physics finite-element solver
8 (COMSOL) is used to simulate the thermal sensing performances of TE fiber in a steady-state
9 based on thermoelectrics modules, and evaluate the flexibility of TE fiber with its deflection
10 based on solid mechanics modules. In the simulation, all the parameters and the geometries of
11 the TE fibers are set to be the same as the actual materials, structures, and environments.
12
13
14
15
16
17
18
19
20
21
22
23

24 **ASSOCIATED CONTENT**

25
26
27
28 **Supporting Information.** The Supporting Information is available free of charge on the ACS
29 Publications website at DOI:

30
31
32
33 Mechanical properties for pure PEI fibers; EDX and XRD analysis of TE fiber cores (PDF)
34
35
36

37 **AUTHOR INFORMATION**

38 39 **Corresponding Author**

40
41
42 *E-mail: wei.lei@ntu.edu.sg
43
44

45 **Author Contributions**

46
47
48 §These authors contributed equally.
49
50

51 **Notes**

52
53
54 The authors declare no competing financial interest.
55
56
57
58
59
60

ACKNOWLEDGMENT

This work is supported in part by the Singapore Ministry of Education Academic Research Fund Tier 2 (MOE2015-T2-1-066 and MOE2015-T2-2-010), Singapore Ministry of Education Academic Research Fund Tier 1 (RG85/16), and Nanyang Technological University (Start-up Grant M4081515: Lei Wei). Authors from Rennes acknowledges the European Commission's H2020-MSCA grant (GA. 642557, CoACH-ETN).

REFERENCES

- (1) Bayindir, M.; Abouraddy, A. F.; Arnold, J.; Joannopoulos, J. D.; Fink, Y. Thermal-Sensing Fiber Devices by Multimaterial Codrawing. *Adv. Mater.* **2006**, *18*, 845-849.
- (2) Oh, J. H.; Hong, S. Y.; Park, H.; Jin, S. W.; Jeong, Y. R.; Oh, S. Y.; Yun, J.; Lee, H.; Kim, J. W.; Ha, J. S. Fabrication of High-Sensitivity Skin-Attachable Temperature Sensors with Bioinspired Microstructured Adhesive. *ACS Appl. Mater. Interfaces* **2018**, *10* (8), 7263-7270.
- (3) Shin, S.-H.; Park, D. H.; Jung, J.-Y.; Lee, M. H.; Nah, J. Ferroelectric Zinc Oxide Nanowire Embedded Flexible Sensor for Motion and Temperature Sensing. *ACS Appl. Mater. Interfaces* **2017**, *9*, 9233-9238.
- (4) Xue, F.; Zhang, L.; Tang, W.; Zhang, C.; Du, W.; Wang, Z. L. Piezotronic Effect on ZnO Nanowire Film Based Temperature Sensor. *ACS Appl. Mater. Interfaces* **2014**, *6*, 5955-5961.
- (5) Webb, R. C.; Bonifas, A. P.; Behnaz, A.; Zhang, Y.; Yu, K. J.; Cheng, H.; Shi, M.; Bian, Z.; Liu, Z.; Kim, Y.-S. Ultrathin Conformal Devices for Precise and Continuous Thermal Characterization of Human Skin. *Nat. Commun.* **2013**, *12*, 938.
- (6) Zhao, D.; Fabiano, S.; Berggren, M.; Crispin, X. Ionic Thermoelectric Gating Organic Transistors. *Nat. Commun.* **2017**, *8*, 14214.

- 1
2
3 (7) Zhang, F.; Zang, Y.; Huang, D.; Di, C.-a.; Zhu, D. Flexible and Self-Powered
4 Temperature-Pressure Dual-Parameter Sensors Using Microstructure-Frame-Supported Organic
5 Thermoelectric Materials. *Nat. Commun.* **2015**, *6*, 8356.
6
7
8
9
10 (8) Hammock, M. L.; Chortos, A.; Tee, B. C. K.; Tok, J. B. H.; Bao, Z. 25th Anniversary
11 Article: The Evolution of Electronic Skin (E-Skin): A Brief History, Design Considerations,
12 and Recent Progress. *Adv. Mater.* **2013**, *25*, 5997-6038.
13
14
15
16
17 (9) Ren, X.; Pei, K.; Peng, B.; Zhang, Z.; Wang, Z.; Wang, X.; Chan, P. K. A Low-
18 Operating-Power and Flexible Active-Matrix Organic-Transistor Temperature-Sensor Array.
19 *Adv. Mater.* **2016**, *28*, 4832-4838.
20
21
22
23
24 (10) Zhang, T.; Li, K.; Zhang, J.; Chen, M.; Wang, Z.; Ma, S.; Zhang, N.; Wei, L. High-
25 Performance, Flexible, and Ultralong Crystalline Thermoelectric Fibers. *Nano Energy* **2017**,
26 *41*, 35-42.
27
28
29
30
31 (11) Zhang, T.; Li, K.; Li, C.; Ma, S.; Hng, H. H.; Wei, L. Mechanically Durable and Flexible
32 Thermoelectric Films from PEDOT: PSS/PVA/Bi_{0.5}Sb_{1.5}Te₃ Nanocomposites. *Adv. Electron.*
33 *Mater.* **2017**, *3*, 1600554.
34
35
36
37
38 (12) Zhang, T.; Wu, S.; Xu, J.; Zheng, R.; Cheng, G. High Thermoelectric Figure-of-Merits
39 from Large-Area Porous Silicon Nanowire Arrays. *Nano Energy* **2015**, *13*, 433-441.
40
41
42
43 (13) Van Herwaarden, A.; Sarro, P. Thermal Sensors Based on the Seebeck Effect. *Sens.*
44 *Actuators* **1986**, *10*, 321-346.
45
46
47 (14) Mzerd, A.; Tcheliobou, F.; Sackda, A.; Boyer, A. Improvement of Thermal Sensors
48 Based on Bi₂Te₃, Sb₂Te₃ and Bi_{0.1}Sb_{1.9}Te₃. *Sens. Actuators A Phys.* **1995**, *47*, 387-390.
49
50
51
52
53
54
55
56
57
58
59
60

- 1
2
3 (15) Lucas, P.; Conseil, C.; Yang, Z.; Hao, Q.; Cui, S.; Boussard-Plédel, C.; Bureau, B.;
4 Gascoin, F.; Caillaud, C.; Gulbiten, O. Thermoelectric Bulk Glasses Based on the Cu–As–Te–
5 Se System. *J. Mater. Chem. A* **2013**, *1*, 8917-8925.
6
7
8
9
10 (16) Cui, S.; Boussard-Plédel, C.; Calvez, L.; Rojas, F.; Chen, K.; Ning, H.; Reece, M.;
11 Guizouarn, T.; Bureau, B. Comprehensive Study of Tellurium Based Glass Ceramics for
12 Thermoelectric Application. *Adv. Appl. Ceram.* **2015**, *114*, S42-S47.
13
14
15
16
17 (17) Srinivasan, B.; Cui, S.; Prestipino, C.; Gellé, A.; Boussard-Plédel, C.; Ababou-Girard, S.;
18 Trapananti, A.; Bureau, B.; Di Matteo, S. Possible Mechanism for Hole Conductivity in Cu–
19 As–Te Thermoelectric Glasses: A XANES and EXAFS Study. *J. Phys. Chem. C* **2017**, *121*,
20 14045-14050.
21
22
23
24
25
26 (18) Abouraddy, A.; Bayindir, M.; Benoit, G.; Hart, S.; Kuriki, K.; Orf, N.; Shapira, O.; Sorin,
27 F.; Temelkuran, B.; Fink, Y. Towards Multimaterial Multifunctional Fibres that See, Hear,
28 Sense and Communicate. *Nat. Mater.* **2007**, *6*, 336-347.
29
30
31
32
33 (19) Stolyarov, A. M.; Wei, L.; Shapira, O.; Sorin, F.; Chua, S. L.; Joannopoulos, J. D.; Fink,
34 Y. Microfluidic Directional Emission Control of an Azimuthally Polarized Radial Fibre Laser.
35 *Nat. Photonics* **2012**, *6*, 229-233.
36
37
38
39
40 (20) Zhang, J.; Li, K.; Zhang, T.; Buenconsejo, P. J. S.; Chen, M.; Wang, Z.; Zhang, M.;
41 Wang, Z.; Wei, L. Laser-Induced In-Fiber Fluid Dynamical Instabilities for Precise and
42 Scalable Fabrication of Spherical Particles. *Adv. Funct. Mater.* **2017**, *27*, 1703245.
43
44
45
46
47 (21) Gumennik, A.; Wei, L.; Lestoquoy, G.; Stolyarov, A. M.; Jia, X.; Rekemeyer, P. H.;
48 Smith, M. J.; Liang, X.; Grena, B. J.-B.; Johnson, S. G. Silicon-In-Silica Spheres via Axial
49 Thermal Gradient In-Fibre Capillary Instabilities. *Nat. Commun.* **2013**, *4*, 2216.
50
51
52
53
54
55
56
57
58
59
60

- 1
2
3 (22) Canales, A.; Jia, X.; Froriep, U. P.; Koppes, R. A.; Tringides, C. M.; Selvidge, J.; Lu, C.;
4 Hou, C.; Wei, L.; Fink, Y. Multifunctional Fibers for Simultaneous Optical, Electrical and
5
6 Chemical Interrogation of Neural Circuits in Vivo. *Nat. Biotechnol.* **2015**, *33*, 277-284.
7
8
9
10 (23) Wei, L.; Hou, C.; Levy, E.; Lestoquoy, G.; Gumennik, A.; Abouraddy, A. F.;
11
12 Joannopoulos, J. D.; Fink, Y. Optoelectronic Fibers via Selective Amplification of In-Fiber
13
14 Capillary Instabilities. *Adv. Mater.* **2017**, *29*, 1603033.
15
16
17 (24) Wang, S.; Zhang, T.; Li, K.; Ma, S.; Chen, M.; Lu, P.; Wei, L. Flexible Piezoelectric
18
19 Fibers for Acoustic Sensing and Positioning. *Adv. Electron. Mater.* **2017**, *3*, 1600449.
20
21
22 (25) Shabahang, S.; Tao, G.; Kaufman, J. J.; Qiao, Y.; Wei, L.; Bouchenot, T.; Gordon, A.P.;
23
24 Fink, Y.; Bai, Y.; Hoy, R. S.; Abouraddy, A. F. Controlled Fragmentation of Multimaterial
25
26 Fibres and Films via Polymer Cold-Drawing. *Nature* **2016**, *534*, 529-533.
27
28
29 (26) Hou, C.; Jia, X.; Wei, L.; Stolyarov, A. M.; Shapira, O.; Joannopoulos, J. D.; Fink, Y.
30
31 Direct Atomic-Level Observation and Chemical Analysis of ZnSe Synthesized by In Situ High-
32
33 Throughput Reactive Fiber Drawing. *Nano Lett.* **2013**, *13*, 975-979.
34
35
36
37
38
39
40
41
42
43
44
45
46
47
48
49
50
51
52
53
54
55
56
57
58
59
60

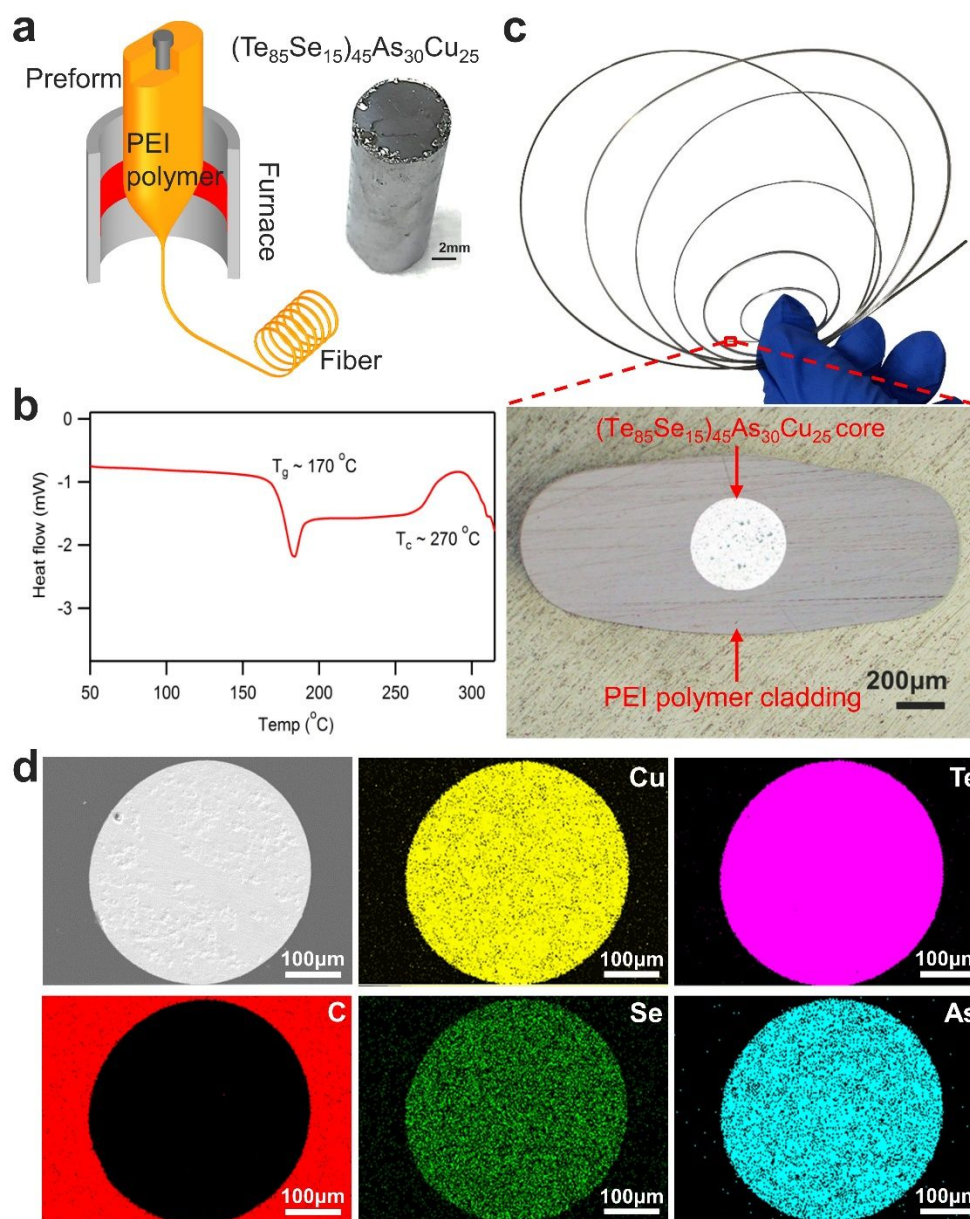


Figure 1. Flexible and long TE fiber fabricated by thermal drawing. (a) Schematic diagram of the drawing process of a TE fiber from the semiconducting glass rod and PEI polymer. (b) Glass transition temperature (T_g) and crystallization temperature (T_x) of the semiconducting glass measured by differential scanning calorimeter. (c) Single TE fiber with good flexibility and the optical microscope image of fiber cross-section. (d) EDX mappings of the cross-section of the TE fiber with the core diameter of $400\mu\text{m}$.

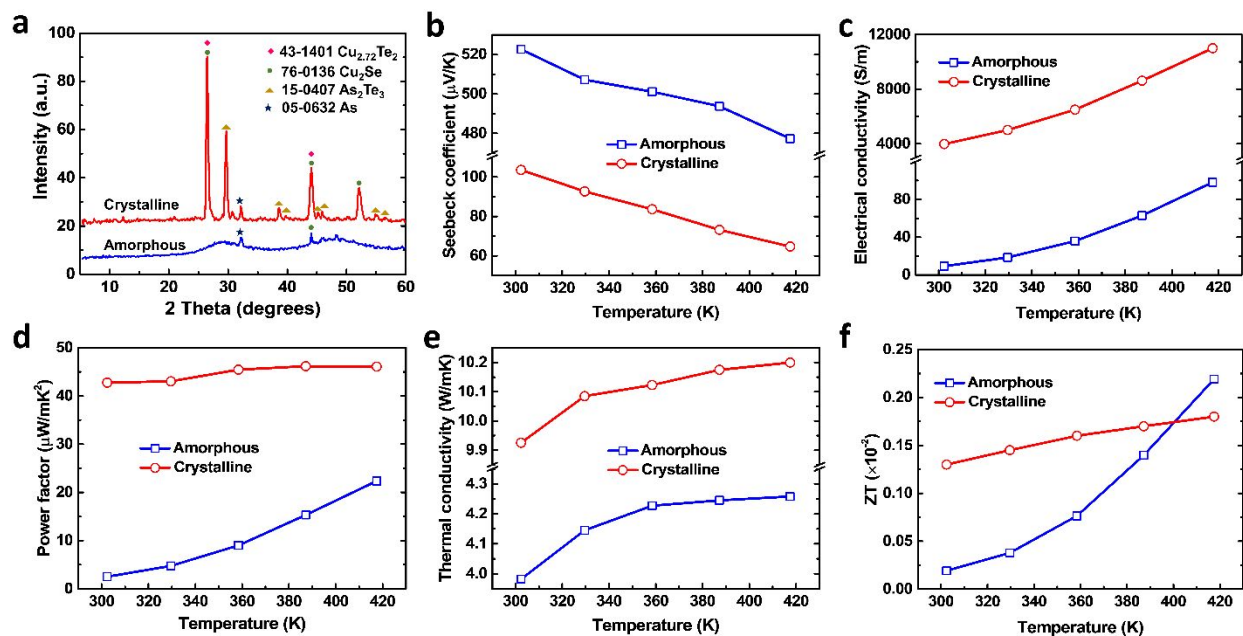


Figure 2. TE properties of the semiconducting glass core with amorphous and crystalline states.

(a) XRD spectrums, (b) Seebeck coefficients, (c) electrical conductivities, (d) power factors, (e) thermal conductivities, and (f) TE figure of merits ZT at different temperatures.

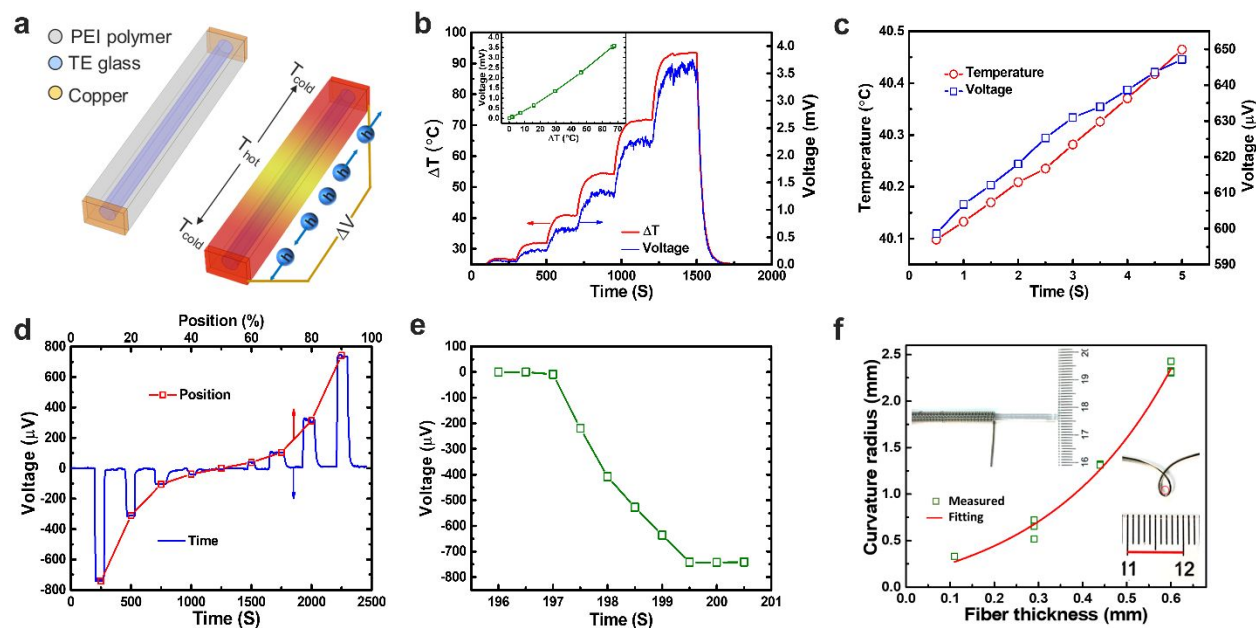


Figure 3. Thermal sensing performance of a single TE fiber. (a) Schematic of the measuring principle for the thermal sensing performance of the TE fiber. (b) Real-time recording the temperature of the heat source located at the 20% length of the whole fiber via the corresponding output voltage from the temperature difference at two fiber ends. (c) The temperature resolution of the TE fiber thermal sensor. (d) Real-time output voltages from the different positions of the thermal source by finger touching. (e) The sensitivity of the TE fiber thermal sensor via finger touching. (f) Minimum curvature radius of TE fibers with different fiber thicknesses, and the inset exhibits that the TE fiber is flexible enough to be wrapped on the surface of a 3 mm diameter silica rod.

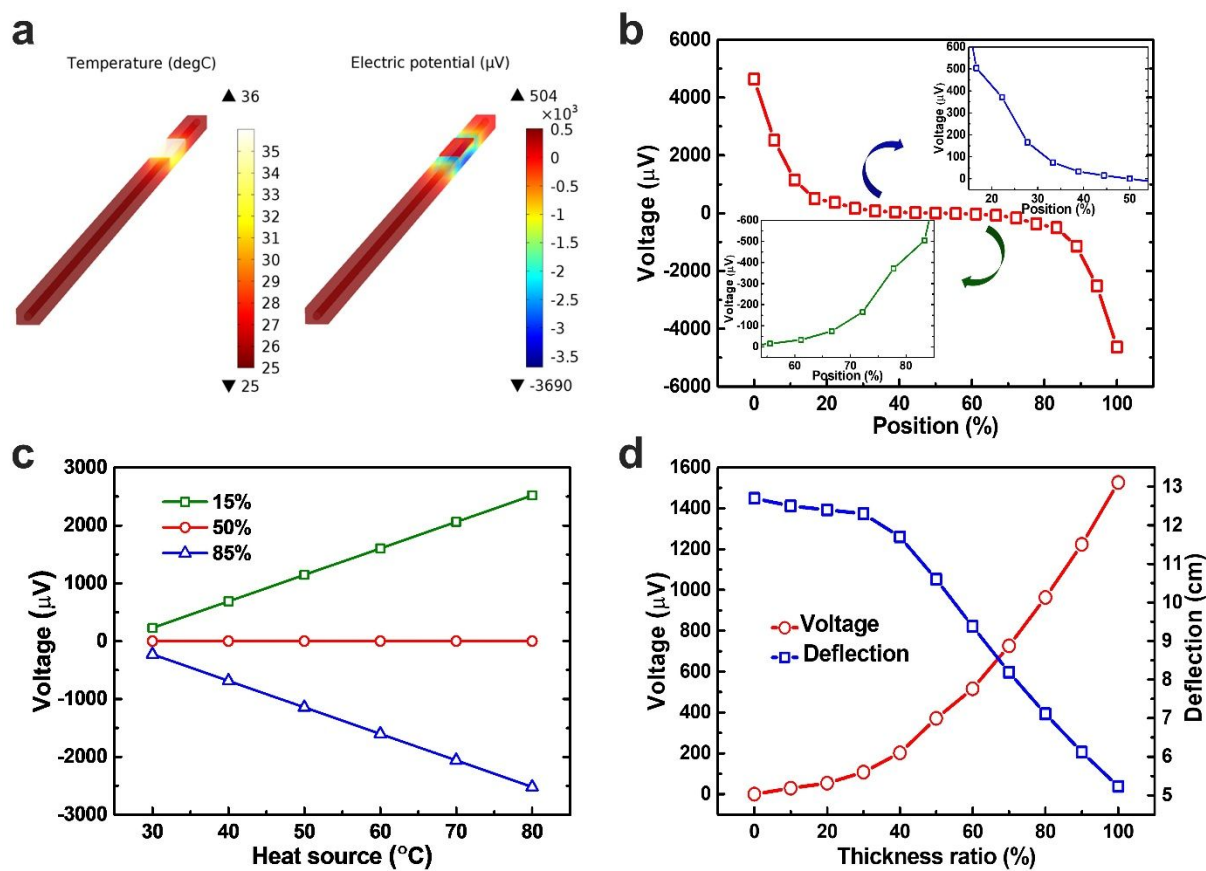


Figure 4. Finite element simulation of the thermal sensing and flexible performance of TE fibers. (a) The simulated results of temperature gradient and electric potential distribution on a single TE fiber. (b) The output voltages vary with the heat source of 36 $^{\circ}\text{C}$ moving along the fiber length. (c) The output voltages induced by different temperatures of heat source at middle point, 15% and 85% fiber length points, respectively. (d) The simulated output voltages and deflections of the fiber thermal sensor for different thickness ratios between the semiconducting glass core and the entire fiber.

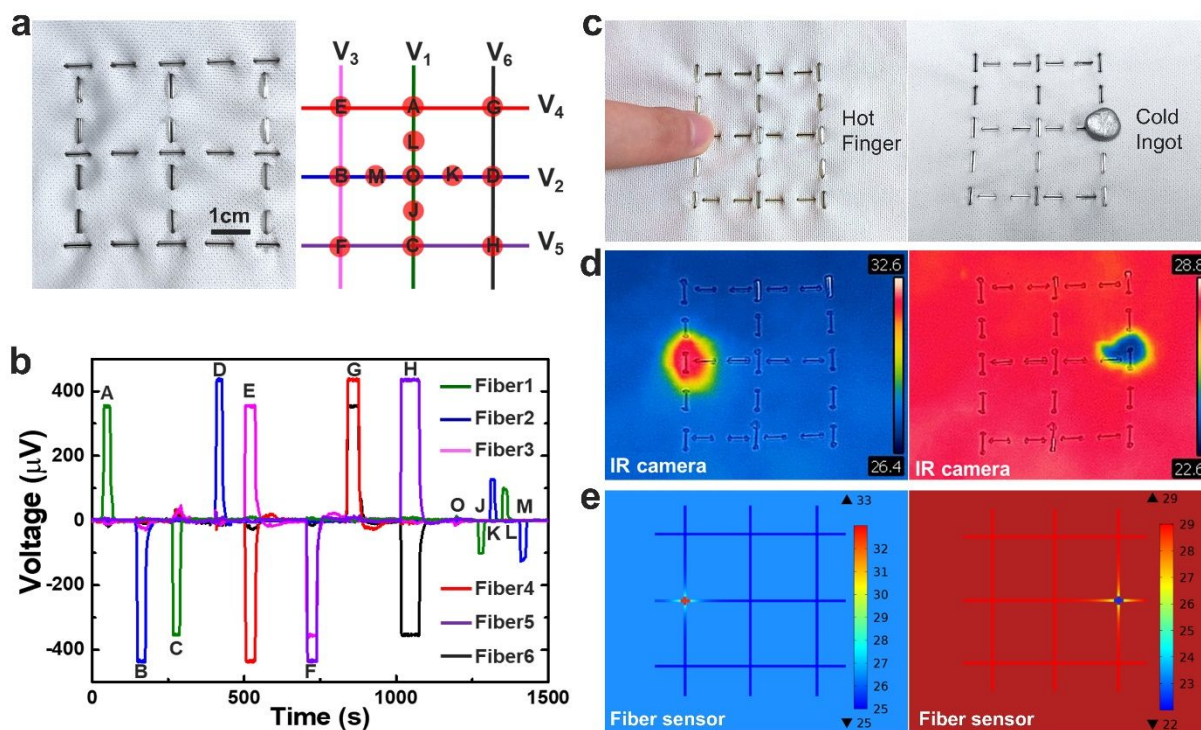


Figure 5. Flexible thermal sensor network based on a 3×3 TE fiber array for simultaneous thermal source detection and positioning. (a) A 3×3 TE fiber array woven into a flexible fabric (left image) and the finger touching points schematically marked by capital letters (right image). (b) The corresponding output voltages of the thermal sensor network for different thermal source positions when finger touches the marked points. (c) Two working situations: finger heating with the temperature of 33 °C and ingot cooling with the temperature of 22 °C detected by (d) thermal IR images taken by an IR camera and (e) reconstructed thermal maps using the data obtained from the fiber array.

TOC Figure:

